Hybrid Imaging System for Simultaneous Spiral MR and X-ray (MRX) Scans

LARS GJESTEBY[1], YAN XI[1], MANNUDEEP K. KALRA[2], QINGSONG YANG[1], AND GE WANG[1], (Fellow, IEEE)

[1]Biomedical Imaging Center, Department of Biomedical Engineering, Rensselaer Polytechnic Institute, Troy, NY 12180, USA
[2]Department of Imaging, Massachusetts General Hospital, Boston, MA 02114, USA

Corresponding author: Ge Wang (ge-wang@ieee.org)

ABSTRACT The needs and the feasibility of simultaneous computed tomography (CT) and magnetic resonance imaging (MRI) were recently reported. In this paper, a spiral magnetic resonance X-ray CT (MRX) imaging system is proposed for head and extremities imaging, which serves as a simple, cost-effective solution on the path to a full-scale CT-MRI fusion. While MRI and X-ray radiography were integrated before, we propose novel designs to acquire simultaneous CT and MR views for synchronized radiographic imaging or joint tomographic reconstruction. Our preliminary permanent magnet configurations achieve a magnetic field strength between 0.1 and 0.2 T while keeping weight low enough for portability. We have also shown that a field strength up to 0.35 T is achievable with permanent magnets that maintain a compact profile, though increased weight would hinder ease of transportation. Simulation results of a joint tomographic reconstruction scheme show the advantage of simultaneously acquired images. The proposed MRX system performs double helical scans in CT and MRI mechanisms, and has multiple niche applications, such as medical imaging on disaster sites, in battle fields, and for under-developed regions.

INDEX TERMS X-ray radiography, CT, MRI, spiral scanning, joint image reconstruction.

I. INTRODUCTION

The case for combining computed tomography (CT) and magnetic resonance imaging (MRI) into a single unit for simultaneous imaging has been recently strengthened [1]. Although a functional prototype has yet to be realized, analysis and improvements on the engineering feasibility continue to progress [2]–[4]. The main challenges that impede the fusion of CT and MRI are the size conflict between hardware components and electromagnetic interferences, such as the magnetic field-induced electron deflection in the x-ray tube [5]. However, low-field MRI minimizes the fringe magnetic field that affects x-ray components and is viable for producing clinically useful images [6], [7]. Furthermore, compressed sensing and interior tomography principles enable the use of smaller hardware components and fewer projections for local image reconstruction, which facilitates simultaneous CT-MRI [8], [9]. A spiral magnetic resonance x-ray CT (MRX) system for head and extremities imaging is proposed here as a simple, cost-effective solution on the path to full-scale CT-MRI fusion.

Projection-based conventional x-ray radiography has wide-ranging applications in modern medical practice. It has come to represent an indispensable part of patient work-up spanning from acute to chronic conditions and cancers, as well as from infectious to trauma-related applications. The low cost, low radiation dose, widespread availability, and rapid, often bedside acquisition have made it the most commonly used imaging technique over the past 100 years. Despite these advantages, conventional radiography remains a modality with two-dimensional projection data from three-dimensional anatomy, as well as one with significantly limited soft tissue contrast resolution. Other cross-sectional imaging techniques such as CT and MRI have 3D capabilities and superior contrast resolution. While CT scanning is associated with higher radiation dose as compared to conventional radiography, the volumetric capability is greatly beneficial. MRI does not involve any ionizing radiation and delivers superior contrast resolution compared to CT. However, unlike CT, the application of MR for determining fracture fragments and their alignment cannot be reliably obtained.

These individual shortcomings make the harmonization of CT and low-strength MRI highly attractive.

The integration of MRI and x-ray technology for hybrid imaging has been previously reported. In 2001, an x-ray tube and a detector array were placed inside an intraoperative MRI scanner, and high-quality images were acquired with both modalities [10]. The study experimentally quantified the interferences among the magnetic field, RF coils, an x-ray source, and a detector, and it was determined that the resulting image distortion was insignificant after minimal adaption of the x-ray hardware. Our system design assumes similar conditions, and similar measures will be taken to minimize the conflicts.

The primary innovation of our scanner is to employ smaller-scale simultaneous spiral CT and MRI to achieve simultaneous radiographic imaging and joint tomographic reconstruction. Spiral scanning is preferred due to its ability to acquire higher quality images for a given level of radiation dose or a given size of a dataset [11].

The MRX scanner is specifically designed for head and extremities imaging to reduce the cost and dimensions of the magnet. A compact profile allows for ease of transportation while enabling high-quality images over regions of interest. Permanent magnets are put forth as the primary means for generating the main magnetic field needed for MRI. We specifically evaluate Halbach configurations of permanent magnets based on prior works that achieve various patterns of homogeneous magnetic fields by radial polarization arrangements of magnet blocks [12], [13]. These arrays maximize the field at the center of the blocks while minimizing the fringe field outside. Permanent magnets are less expensive than the superconducting magnets employed in the standard clinical units, which require liquid nitrogen or helium maintained at extremely cold "critical" temperatures to nullify the electrical resistance of the wire. This complexity does not facilitate movability, and operation costs are high. Since permanent magnets have an always-present magnetic field and do not need a power source to generate the field, they are much easier to maintain while the only obstacle to mobility is weight of the material. Another drawback of permanent magnets is that the field cannot be shut off so ferromagnetic metal would have to be kept away from the scanner. Simple resistive magnet coils are a potential alternative to both permanent and superconducting magnets, as they are less expensive than superconductors, and their field can be shut off. However, the high amount of current needed to generate clinically relevant fields makes resistive magnets unrealistic for MRX at this moment.

The design and development of a combined simultaneous, compact spiral CT-MRI system targets several applications. The most evident is for assessing trauma, specifically of the extremities, spine, or head, so that images can be acquired rapidly with minimal patient movement. MRX is also a way to improve medical imaging in developing countries that do not have wide access to advanced equipment. An inexpensive, compact scanner that performs both CT and MRI can bring essential help to regions that have been without either modality thus far.

The purpose of this work is to suggest the novel concept, design criteria, and applications of a portable simultaneous x-ray and MR imaging system, show simulation results for the technical feasibility, and discuss relevant issues and potential solutions for spiral MRX. The following section describes the physical principles of spiral CT and MRI, which are combined in the MRX system to acquire 3D volumetric views over a short period of time with complementary functional and anatomical information. The third section details hardware considerations for the cost and movability of the imaging unit. The fourth section presents several permanent magnet designs with the x-ray components, simulates the fields that can be practically generated, and demonstrates joint tomographic image reconstruction. The final section discusses the important applications of the MRX system and the next steps towards its development.

II. PHYSICAL PRINCIPLES

In digital radiography, x-ray photons are directed from an x-ray tube toward a patient and are absorbed, scattered, or transmitted to a detector array. A flat panel detector array measures the intensity of x-rays received at each pixel, and converts this quantity into light or an electrical signal. The digital output resulting from the analog signal is used to form raw data. Spiral CT acquires views at many angles as the source rotates around the patient being translated through the gantry. The hardware of this subsystem is relatively straightforward as compared to MRI, and thus the bulk of the feasibility analysis for the MRX system is focused on the MRI aspects.

Typical clinical MRI scanners contain a magnet with a field strength in the range of 1 to 3 T [14]. In humans, MRI systems target hydrogen protons to acquire signal. When the proton spins are in the magnetic field of a scanner, they tend to be aligned along the axis of the field. The hydrogen atoms can orientate either parallel or antiparallel to the main field direction, and there will be slightly more spins lined up in the parallel direction, creating a net magnetization vector. The magnetization vector precesses around the field axis at a frequency (ω_0) that is dependent on the strength of the magnetic field (β_0) and a constant gyromagnetic ratio (γ):

$$w_0 = \gamma B_0 \qquad (1)$$

To perturb this precession, a radio frequency (RF) pulse at the resonant frequency of the hydrogen protons, known as the Larmor frequency, is applied to an area of the body to be imaged. The gyromagnetic ratio for hydrogen is 42.57 MHz/T, so the Larmor frequency of hydrogen protons in a 1 T field is 42.57 MHz. Typically, the RF pulse is shut off when the magnetization vector falls 90° from the original direction. After this point, the hydrogen atoms relax back to their steady state in the magnetic field. During this relaxation, energy released by the protons results in a signal that can be detected by the RF coil. Various pulse sequences are used depending on the imaging application.

MRI images are formed by pinpointing the spatial location of proton groups that are spinning at different rates. To achieve this, gradient coils are employed in combination for slice selection, frequency encoding, and phase encoding. When turned on, the gradient coils alter the strength of the homogeneous main magnetic field linearly along the x-, y-, and/or z-directions so that protons precess at various frequencies within different time windows depending on their locations in the gradient field. An alternative method for encoding is to instead take advantage of slight non-uniformities in the main magnetic field so that field strength naturally varies with location in the imaging field of view [15]. This would eliminate some hardware. Either way, the signals acquired by the RF coil give information in the Fourier domain for image reconstruction. The principle of interior tomography enables small regions of interest to be reconstructed with less data than necessary for global reconstruction. For MRI, this means that the homogeneous magnetic field area can be focused only on a specific region to be imaged.

III. MRX SYSTEM COMPONENTS

The desired specifications of the MRX system are as follows: low weight for portability, low power for efficiency, a homogeneous main magnetic field over the imaging region, a clinically-relevant main magnetic field strength, and minimal fringe fields. To achieve these conditions, several system components are analyzed.

A. MAIN MAGNETIC FIELD

The main magnetic field for clinical MRI is typically generated by superconducting magnets. When cooled to a critical temperature, these coils have zero electrical resistance and can carry high current density. This allows for a high magnetic field to be efficiently achieved. Despite these advantages, superconducting magnets are expensive to build and require liquid nitrogen or helium. In addition, they typically weigh several thousand kilograms. While superconducting magnets are the best option for generating the ideal magnetic field, they prohibit portability and are incompatible with the requirements for a low-cost, compact MRX system.

Alternatives for generating the main magnetic field are permanent magnets and resistive magnets. Permanent magnets for MRI have the advantage over electromagnets of not needing an electric current. The material of the magnet, a rare-earth metal, produces an ever-present field, thus removing power consumption and thermal dissipation concerns for the subsystem. The Halbach arrays can be designed to produce a strong field at the center of the magnet configuration while keeping the external fringe field low.

Resistive magnets are electromagnets through which a strong electric current is passed. A magnetic field inside the coil is proportional to the intensity of the electric current supplied. The advantage of this setup is that the field can be removed by turning off the power supply. However, large amounts of current are needed to achieve clinically relevant field strengths. The material and design of the coil can be altered for various field strengths, such as by wrapping a wire around an iron core instead of a hollow container, or constructing a Bitter magnet solenoid. Bitter magnets are built by stacking circular copper plates in a helical configuration with insulating spacers [16]. Due to power consumption and heat generation of large-scale resistive magnets, cooling systems must be integrated. Bitter plates are designed with many holes to allow water to circulate through the stack to control temperature. Although these engineering adjustments improve the viability of resistive magnets, permanent magnets are deemed to be preferable for the specifications of the MRX system. If zero resistance of superconducting coils could be achieved at higher temperatures without the need for cryogenic cooling, then the case for superconducting/resistive magnets would become stronger.

B. SUPERCAPACITORS

If the imaging unit were made portable, x-ray radiography with MR could assess fractures, bone contusions, and internal bleeding directly in disaster areas or at a patient's bedside. Such a system could be powered by an onboard supercapacitor array to facilitate mobility. This also means that a patient in critical condition would not have to be transported to an imaging suite, and MRX could remove the need for a higher-dose CT exam and a subsequent independent MRI, allowing for faster treatment decisions.

The feasibility of commercially available supercapacitors as energy storage banks for MRI scanners was demonstrated by Ristic *et al.* [17]. Various pulse sequences were successfully tested with supercapacitors, including *T1* and *T2* spin echoes. Graphene supercapacitors are a developing technology with the highest charge-capacity-to-weight ratio up to 550 F/g [18]. This characteristic is due to its single atomic layer makeup, leading to a high relative surface area for storing charge while minimizing thickness. A recent supercapacitor advancement builds upon the graphene technology and incorporates nitrogen doping of the carbon layers for higher energy storage while maintaining rapid charging and discharging rates. This material can achieve a capacitance of 855 F/g in aqueous electrolytes [19].

The cost and power requirement of the supercapacitor array is dependent on the type of magnets used in the system and the field strength needed. Since resistive magnets consume the most power of all magnet types, opting for permanent magnets would substantially lessen the load. In this case, the power source would only need to support x-ray components, MRI gradient coils, circuitry, and computers.

C. ELECTROMAGNETIC SHIELDING

Another consideration for the MRX system design is the shielding of the magnetic field beyond the region where it is needed to minimize interference with x-ray production. This can be accomplished with a support structure made of a ferromagnetic material, such as steel, through which the magnetic field generated by the electromagnet can complete its path. With steel blocks located at the bottom of the

permanent magnet rings, the residual field will be attracted to this material and minimize the leakage at the top of the gantry. Optimization will be needed to balance the trade-off between added weight and fringe field reduction.

D. CT AND MR IMAGE RECONSTRUCTION

In the MRX system, the CT and MRI subsystems perform measurements simultaneously. Since CT and MRI are hardware-wise independent, image reconstructions can be independently performed in a manner similar to conventional CT and MRI as the bottom line. Furthermore, given the spatially and temporally registered CT and MR measurements obtained by MRX, a combined image reconstruction scheme will benefit both sub-system performances [20]. Here, we propose to adapt the unified CT-MRI image reconstruction scheme to lower the radiation dose of CT and improve the image quality of MRI with a low background magnetic field. The proposed CT-MRI reconstruction method is a learning-based method which learns the relationships between low-resolution CT (or MRI) images and high-resolution CT (or MRI) images.

The first step is to reconstruct CT and MRI images using some conventional methods, such as the simultaneous algebraic reconstruction technique with total variation (SART-TV):

$$\min_{\mathbf{u}_{CT}} \|\mathbf{u}_{CT}\|_{TV}, \quad \text{s.t. } \mathbf{M}\mathbf{u}_{CT} = \mathbf{f}, \tag{2}$$

$$\min_{\mathbf{u}_{MRI}} \|\mathbf{u}_{MRI}\|_{TV}, \quad \text{s.t. } \mathbf{RF}\mathbf{u}_{MRI} = \mathbf{g}, \tag{3}$$

where $\mathbf{u}_{CT}$ and $\mathbf{u}_{MRI}$ are CT and MR images to be reconstructed, $\mathbf{M}$ is a system matrix in CT imaging, $\mathbf{F}$ denotes the Fourier transform, $\mathbf{R}$ is a sampling mask in the k-space, $\mathbf{f}$ and $\mathbf{g}$ are CT and MRI measurements respectively, and $\|\cdot\|_{TV}$ denotes the TV transformation.

Structural coupling and compressive sensing techniques were combined [20], in which each sub-image in CT (or MRI) is represented by paired local CT-MRI structures. That is, the association between target CT and MRI images are naturally established. In the current joint image reconstructions, such an association is extracted using an artificial neural network to guide both CT and MRI reconstructions:

$$\min_{\mathbf{u}_{CT}} (1-\alpha) \|\mathbf{u}_{CT}\|_{TV} + \alpha \|\mathbf{u}_{CT} - \mathbf{u}_{CT}^{est}\|_{TV},$$
$$\text{s.t. } \mathbf{M}\mathbf{u}_{CT} = \mathbf{f}, \tag{4}$$

$$\min_{\mathbf{u}_{MRI}} (1-\alpha) \|\mathbf{u}_{MRI}\|_{TV} + \alpha \|\mathbf{u}_{MRI} - \mathbf{u}_{MRI}^{est}\|_{TV},$$
$$\text{s.t. } \mathbf{RF}\mathbf{u}_{MRI} = \mathbf{g}, \tag{5}$$

where $\mathbf{u}_{CT}^{est}$ and $\mathbf{u}_{MRI}^{est}$ are estimated images using the CT-MRI artificial neural network according to the corresponding CT and MRI images, and α balances contributions from total variation and image similarity respectively. Eq. (2-5) are all well-posed convex optimization problems and can be effectively solved in the split-Bregman framework. The detailed implementation of the unified CT-MRI reconstruction scheme is discussed in our group's previous articles [20], [21]. These algorithms can handle a small degree of inhomogeneity in the B_0 magnetic field by utilizing the interior MRI reconstruction technique, which looks for regions of equal field strength ("level sets") and sufficient gradient to achieve spatial localization [1]. The region of interest can be reconstructed solely with data inside that region, and an accurate solution can be obtained. If the local magnetic field is made homogeneous, interior MRI will be even easier with conventional gradient and RF coils.

IV. SIMULATION RESULTS
A. PERMANENT MAGNET DESIGNS

The most feasible class of magnets for the MRX system is permanent magnets, with its advantages over resistive magnets described in subsection 3.1. Now, we present permanent magnet designs for the main magnetic field. All the illustrations were rendered using the 3D CAD software Solid Edge (*Siemens PLM Software, Plano, Texas*). The configurations were based on the relative arrangement of the magnet hardware, CT hardware, and a patient. The gradient coils and RF coil needed for MRI were omitted in the figures for visual simplicity, but these would also be present in the system surrounding the patient. Designs were simulated to assess magnetic field strengths using FARADAY (*Integrated Engineering Software, Winnipeg, Manitoba*), which is a 3D solver of Maxwell's equations that employs finite element methods.

The ever-present field of permanent magnets eliminates the need for a high current source, but weight is an issue for portability, as the rare-earth metals are dense. The material used in the simulations was NdFeB 45 MGOe Sintered, which is an alloy of neodymium, iron, and boron, and has a density of 7.5 g/cm^3. Fig. 1(a) illustrates two rings of magnets arranged in a simplified Halbach configuration, with each ring containing 8 blocks with the magnetization directions as indicated in Fig. 1(b). The rings have an inner diameter of 30 cm, an outer diameter of 60 cm, and a thickness of 5 cm, and are separated by 20 cm. The total weight of all 16 magnet blocks in both rings is 158 kg. The x-ray hardware is positioned above and below the patient and can be rotated in a full circle while the patient table is translated during spiral CT and MR scanning. A magnetic field on the order of 0.11 T is present in a 10 cm cubic imaging region between the rings, as shown in the front view in Fig. 1(c). Fig. 1(d) displays a side view of the magnetic field in the imaging region. The field can be increased by increasing the volume of the magnets, but this also increases weight, which would hinder the portability of the system. The fringe magnetic field was plotted as shown in Fig 1(e). At a distance of 35 cm above the center of the B_0 field where the x-ray source is located, the field strength is ~0.0064 T, or ~6% of B_0. With steel flux return blocks added at the bottom of the magnet rings, the fringe field strength at the position of the x-ray source is reduced by nearly half, to 0.0034 T, as depicted in Fig 1(f).

One variation is to add a partial third ring between the other two with only the four side magnet blocks to preserve space for the x-ray components, as shown in Fig. 1(g). This addition increases the field strength to ~0.16 T at the center
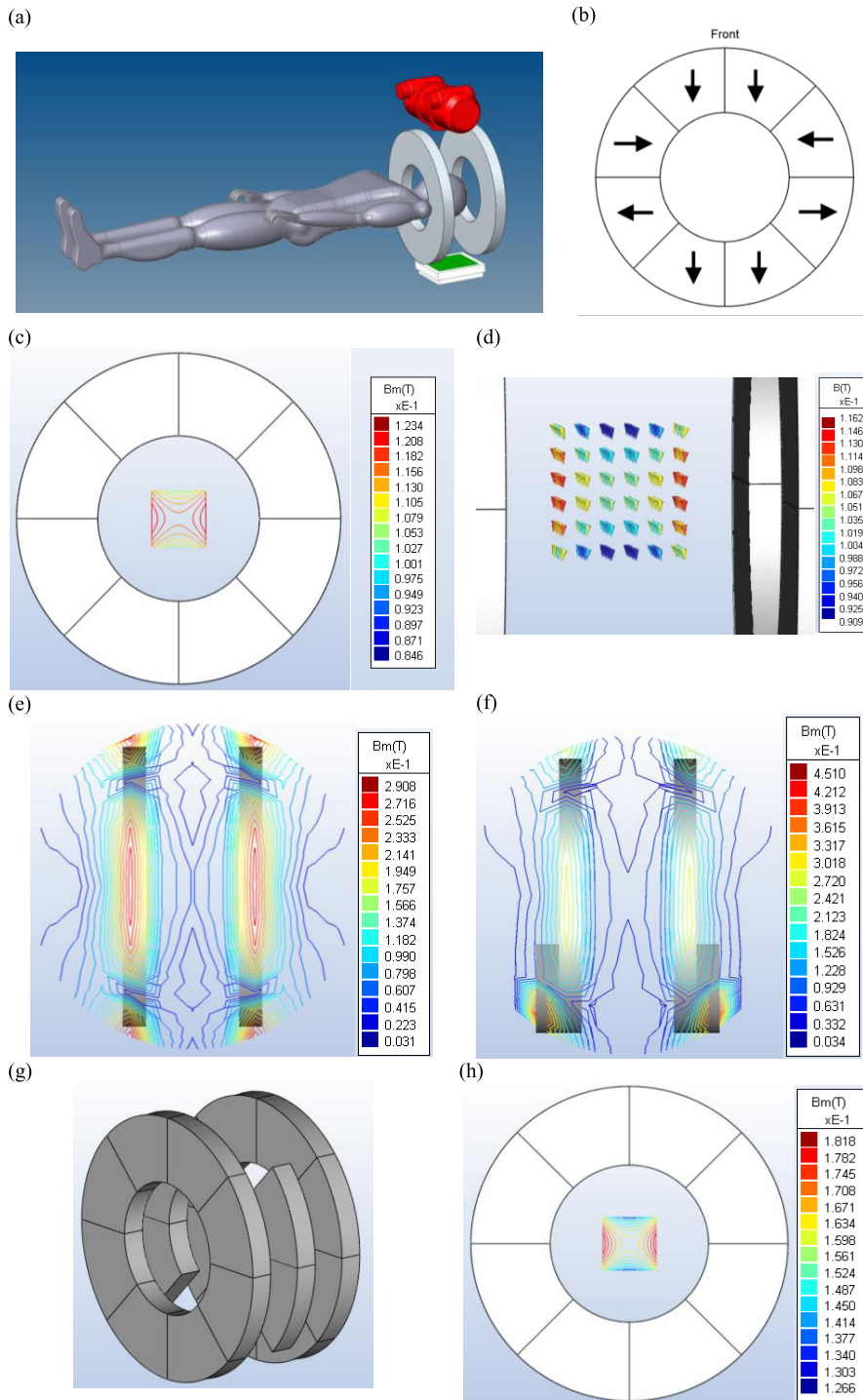
FIGURE 1. Permanent magnet Halbach rings design. (a) The relative arrangement of the magnet rings, x-ray hardware, and patient for simultaneous CT and MRI. (b) The rings each contain 8 block magnets with field polarity indicated by the arrows (front view). (c) A downward magnetic field is produced yielding a strength on the order of 0.11 T in a 10 cm cubic region (front view). (d) The magnetic field arrows in the cubic region as seen from the side view between the rings. The side view of the fringe magnetic field around the gantry is displayed without (e) and with (f) steel return blocks at the bottom. (g) A partial third ring with only the four side magnet blocks is added to increase field strength (isometric view). (h) This results in a stronger magnetic field on the order of 0.16 T in the imaging region (front view).

of the imaging region, as indicated in Fig. 1(h), though the total magnet weight increases to 198 kg. The design may be further optimized to balance field strength and weight.

Another design based on the Halbach arrangement is depicted in Fig. 2(a). The magnet bars above and below the patient are 30 cm wide along the largest dimension and each
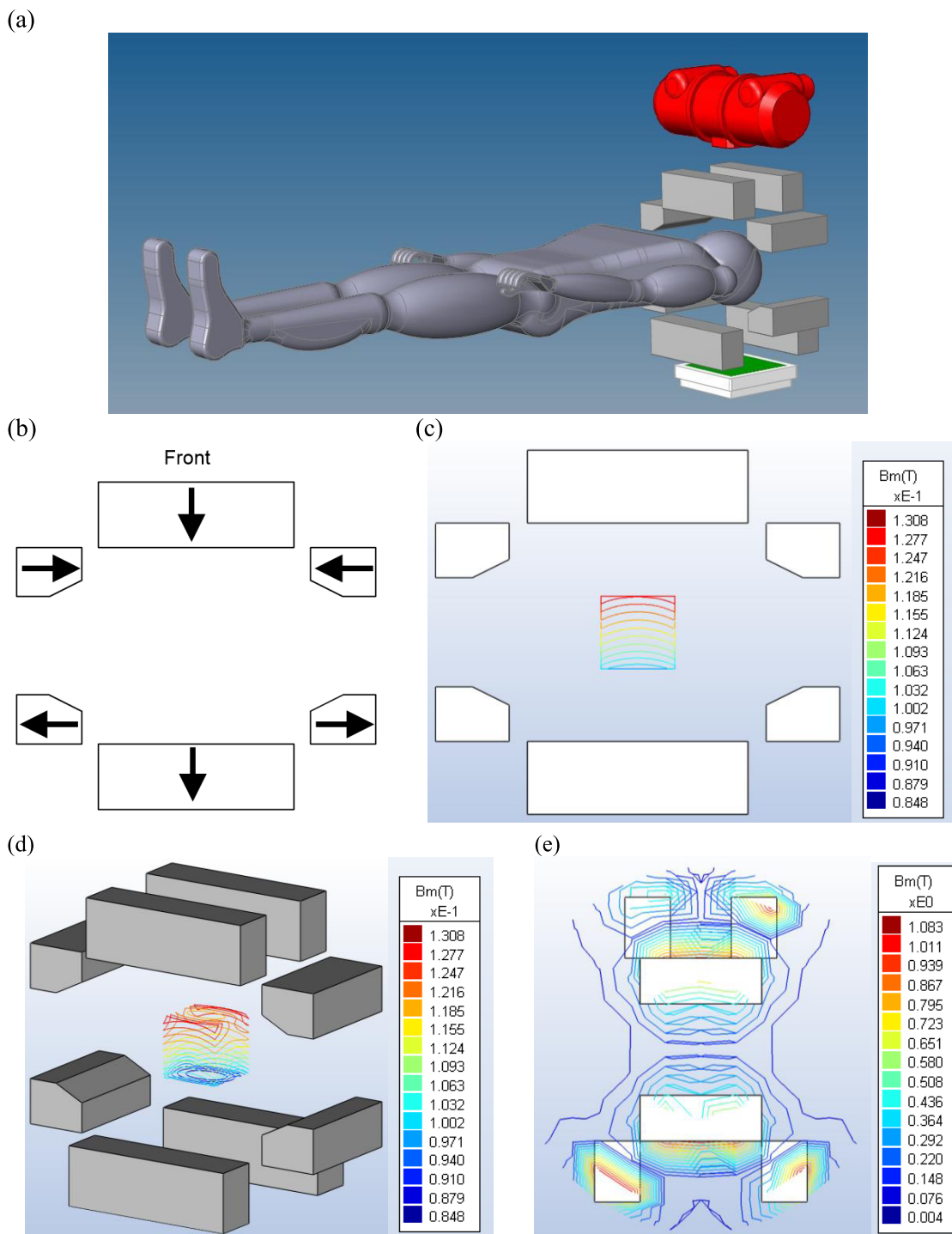
(a)

(b)

Front

(c)

(d)

(e)

FIGURE 2. Permanent magnet Halbach bars design. (a) The relative arrangement of the magnet bars, x-ray hardware, and patient for simultaneous CT and MRI. (b) The bar magnets have field polarities as indicated by the arrows (front view). (c) A downward magnetic field is produced yielding a strength on the order of 0.11 T in a 10 cm cubic region (front view). (d) The magnetic field in the imaging region as seen from an isometric view. (e) The side view of the fringe magnetic field around the gantry.

weigh approximately 17 kg. The two top magnets are separated by 10 cm to allow room for the x-ray tube window. The bottom two magnets are separated by 20 cm to accommodate the flat panel detector. Additionally, there are two pairs of magnet bars flanking either side of the patient measuring

20 cm in length along their largest dimension. Each of these blocks weighs a little over 10 kg, which brings the total weight of the configuration to approximately 109 kg. The magnet polarities of these bars are indicated in Fig. 2(b). A magnetic field on the order of 0.11 T with a natural gradient
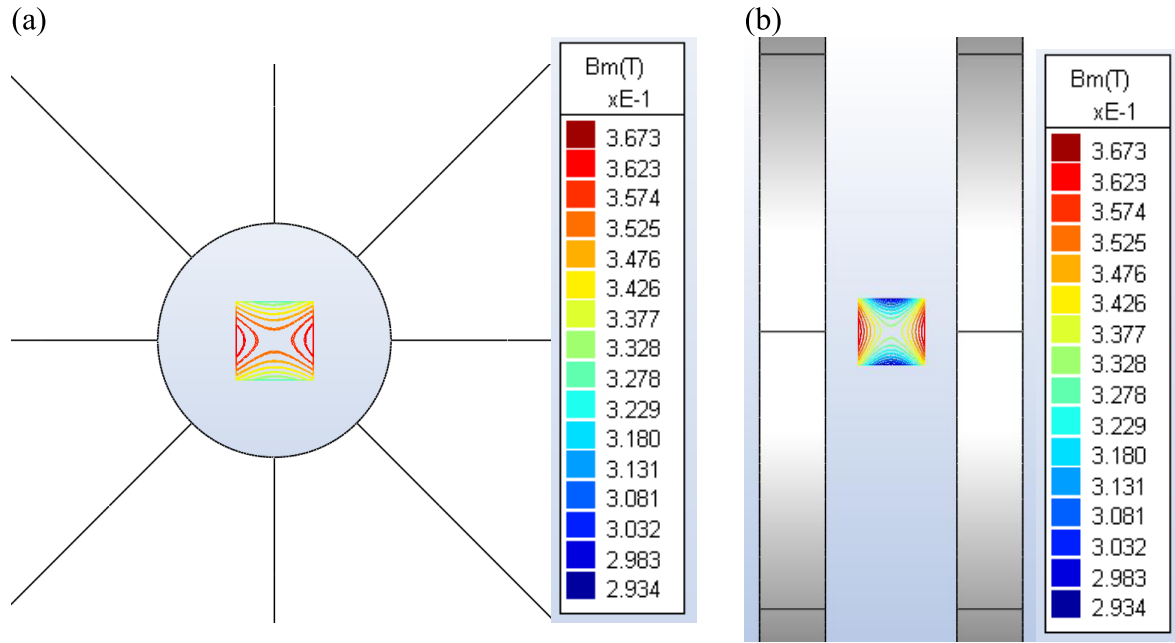
(a)

(b)

FIGURE 3. Alternative design for higher magnetic field strength. (a) A downward magnetic field is produced yielding a strength on the order of 0.34 T in a 10 cm cubic region (front view). (b) The magnetic field in the imaging region as seen from a side view.

TABLE 1. Comparison of the presented magnet designs.

Design	Weight	Central B_0 Field Strength	Homogeneity Deviation Within ROI (approx.)
Fig. 1(a-e)	158 kg	0.11 T	5%
Fig. 1(g-h)	198 kg	0.16 T	10%
Fig. 2	109 kg	0.11 T	20%
Fig. 3	1,589 kg	0.34 T	6%

is present in a 10 cm cube imaging region at the center of the bars, as shown in Fig. 2(c). Fig. 2(d) displays the isometric view of the magnetic field in the imaging region. The fringe magnetic field around the system is plotted in Fig. 2(e). At a distance of 30 cm above the center of the B_0 field where the x-ray source is located, the field strength is $\sim$0.035 T, which is relatively high compared with B_0. A steel return did not have a significant effect on the fringe field in this configuration.

Figures 1 and 2 present compact, lightweight magnet designs that are ideal for a portable spiral MRX system, but the field strength may need to be higher for better image quality in some applications. The field can be increased by expanding the outer diameter and thickness of the magnet rings. Of course, weight will also increase substantially, which hinders the mobility of the scanner. Figure 3 offers an additional two-ring design in the same configuration as Fig. 1(a-d), but with larger ring thicknesses and diameters. Fig. 3(a) and 3(b) show front and side views of the magnetic field, which has a strength of $\sim$0.34 T in a 10 cm cubic region between the rings. The rings have an inner bore diameter

of 30 cm, an outer diameter of 120 cm, and a thickness of 10 cm, and are separated by 20 cm. The total weight of all 16 magnet blocks in both rings is 1,589 kg. For comparison, a commercially available MRI scanner that utilizes superconducting magnets typically weighs at least 7,000 kg. The specifications of the magnet designs presented in this section are summarized in Table 1.

B. IMAGE RECONSTRUCTION
Numerical simulations were performed to evaluate the feasibility of the proposed learning-based CT-MRI reconstruction scheme. In our pilot study, CT and MRI datasets were derived from the Visible Human Project (VHP). An identical human head model was sequentially scanned by CT and MRI scanners. This acquisition process is illustrated in Fig 4. The CT and MR images were pre-processed for spatial registration and voxel normalization. Numerical phantoms used in our experiment are displayed in Fig. 5(a, d) with image size of 212×212 pixels. In our proposed CT-MRI artificial neural network, well-registered CT and MRI images are taken as inputs.
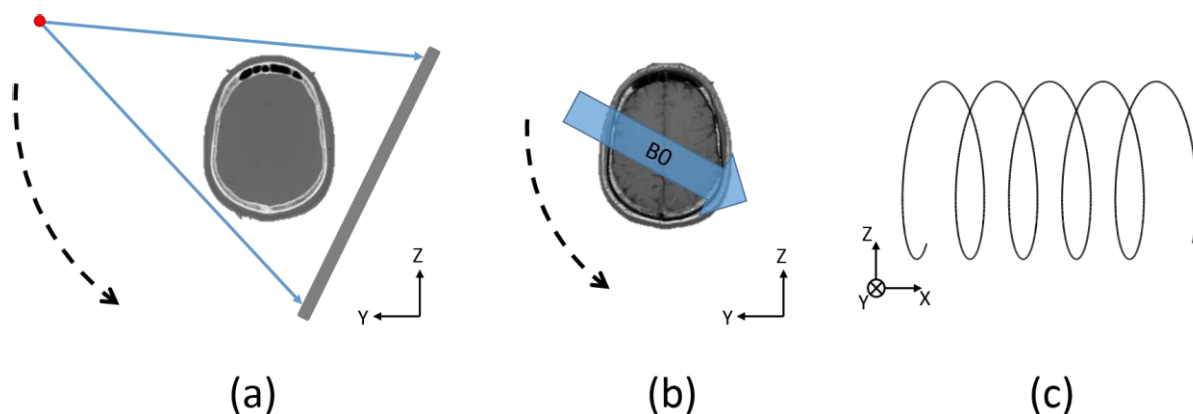
FIGURE 4. Data acquisition with the MRX system. (a) The CT subsystem is similar to a conventional CT scanner in which an x-ray source and a detector array are rotated around the subject. (b) In the MRI subsystem, a spatial encoding magnetic field is achieved by rotating the MR gantry around the subject to obtain generalized projection data. (c) During CT and MRI data acquisition, the MRX system or the subject is also translated longitudinally, thus forming double helical scanning trajectories to cover a long region of interest.
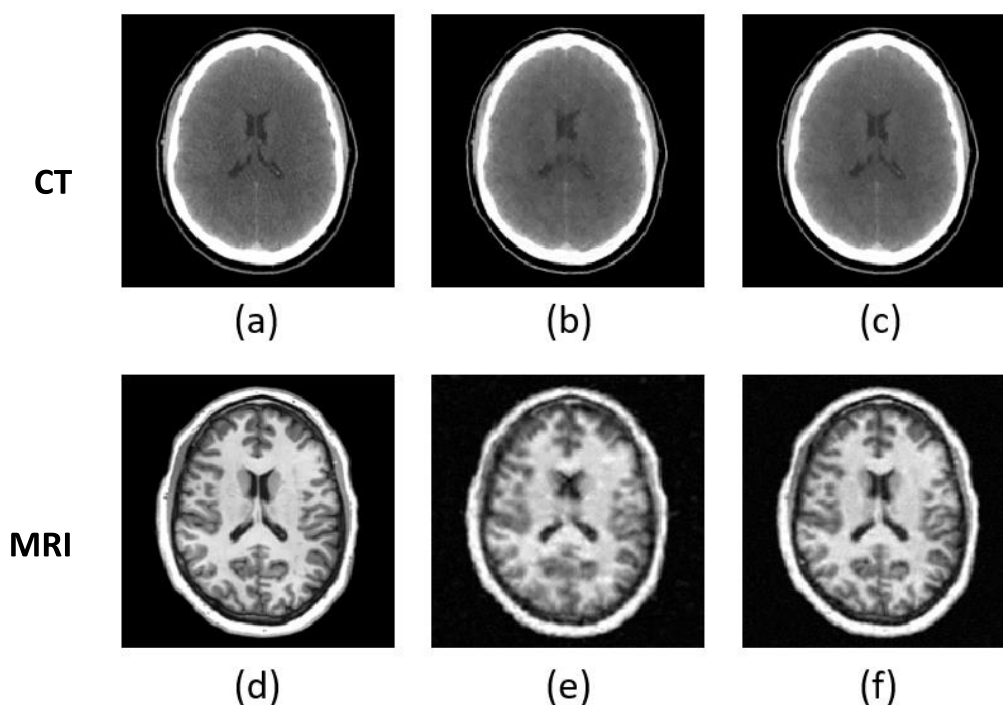

FIGURE 5. Simulation of MRX image reconstruction. CT (a) and MR (d) images from the VHP project serve as the ground truth. In both CT and MR data acquisitions, 30 rotation steps were used. Conventional CT and MR image reconstruction results are displayed in (b) and (e), and their corresponding unified reconstruction results are in (c) and (f), respectively.

In CT imaging, 30 projections were collected around the phantom shown in Fig. 5(a). Due to the concern of x-ray radiation during CT imaging, we aimed to minimize the ionizing radiation level needed while maintaining a suitable image quality. Hence, 30 projections were used in our simulation, which is consistent with the number of views used for sparse-view CT studies in the literature [22]. In MRI scanning, low-field measurement data were obtained in 30 rotation steps (Fig. 5(d)). The B_0 field was slightly inhomogeneous and modeled after a previously reported rotating

Halbach gantry [7]. The average field strength was simulated at 0.08 T to demonstrate the minimum capability of our system. The inhomogeneous B_0 field was treated as a superposition of an ideal homogeneous field and an additional gradient field, and as the B_0 field was rotated, independent data were collected for image reconstruction. The initial CT and MRI reconstructions using the SART-TV method are shown in Fig. 5(b, e). In the joint image reconstruction of the MRX system, a unified scheme was applied in which the CT image and MR image were connected by coupling their
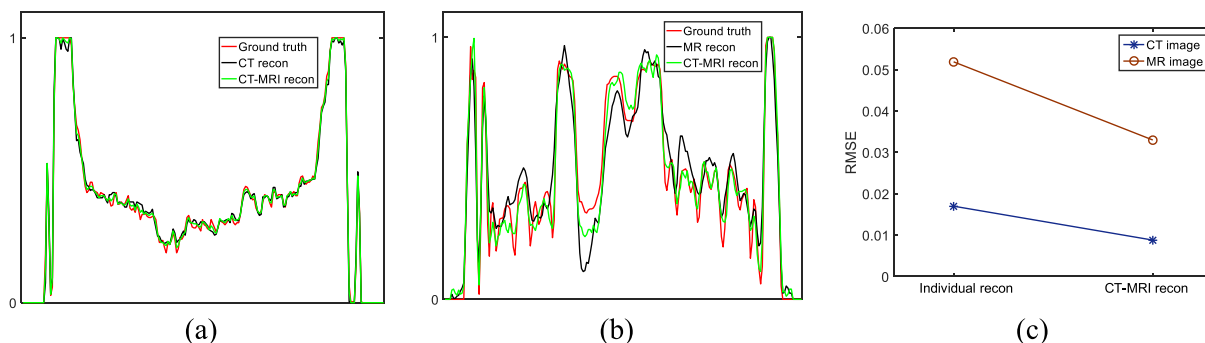
FIGURE 6. Comparison between individual CT/MR reconstructions, unified CT-MRI reconstruction, and ground truth. (a) Line profiles of CT and unified CT-MRI reconstructions. (b) Line profiles of MR and unified CT-MRI reconstructions. (c) RMSE quantifies the reconstruction accuracy relative to the ground truth.

structures to guide each reconstruction. The reconstructed images using our proposed unified CT-MRI scheme are presented in Fig. 5(c, f).

Quantitative comparison of the reconstructed images with the ground truth is presented in Fig. 6, in which vertical line profiles of each resultant image from Fig. 5 are plotted. The root mean squared error (RMSE) was employed to measure the reconstruction accuracy. Fig. 6(c) indicates that the unified CT-MRI reconstruction technique results in less error than individual CT and MRI reconstructions via SART-TV.

V. DISCUSSION

The spiral MRX system described in this work enables the simultaneous acquisition of CT and MRI data for hybrid tomographic imaging of the head, neck, and extremities. Our permanent magnet designs achieve fields between 0.1 and 0.2 T while keeping weight low enough for portability. For extremity imaging, specifically in knees, low-field MRI at 0.2 T has been shown to be clinically viable for diagnosing ligament and meniscus damage [23]. These field strengths are expected to achieve satisfactory image quality for other applications, such as head and spine imaging, though higher fields will yield higher resolution. Hence,we have also shown that field strengths up to 0.35 T are achievable with permanent magnets that keep a compact profile, although increased weight would compromise ease of transportation. The fringe magnetic field at the location of the x-ray source can be greatly reduced by a steel flux return.

The homogeneity of the B_0 magnetic field generated by permanent magnets could be a challenge, but it is achievable in principle. In our designs presented in Fig. 1(a-e), the field strength deviations are about 5% in the imaging region of interest. The previously reported interior MRI reconstruction algorithm can handle slight inhomogeneity in the B_0 field with special pulse sequences and dedicated techniques [1]. However, a homogeneous field in the imaging region of interest makes reconstruction easier. A potential solution to improve our designs is to modify magnetic surfaces and add shimming coils. A recent study demonstrated an improved field homogeneity via dedicated shaping of the magnets [24].

Specifically, the boot surfaces, based on parabolic or hyperbolic functions, modify the magnetic field distribution to maintain a greater homogeneity over a region of interest for imaging. In future work on MRX, we would modify the shape of the magnets and include shimming coils to reduce the field inhomogeneity.

To increase the magnetic field homogeneity, decrease the peripheral field, and optimize the system compactness, high-temperature superconducting wires are a possible future solution in place of permanent magnets [25], [26]. Superconducting wires that have been developed so far are lightweight and thin compared to copper conducting wires, and can accommodate a cryostat line inside the cable [28], [29]. They have a high current-carrying capacity that would allow higher field strengths to be achieved than those from permanent magnets in our lightweight designs. Researchers have been working towards room-temperature superconductors [27], which would hopefully remove the major challenges involved with cryogenic MRI cooling in the future.

A similar alternative design solution is superconducting optical fibers as developed by Gary Pickrell's group. Fibers with lead and tin cores have been tested for superconductivity in a liquid helium bath at 4K [30], [31]. Fibers injected with liquid helium can exhibit superconductivity for an extended period of time while they warm to room temperature [32]. In the context of MRX, superconducting fibers could be wound into coils and used to create a homogeneous local magnetic field on the order of 0.2 T. The conditions for superconductivity are much simpler to achieve than large-scale cryogenic superconducting magnets. Future studies on MRX will focus on implementing this novel technology.

There are several important applications in which the MRX system can be practically useful. For extremity trauma, MRX can deliver both bone information from CT and soft tissue information from MR. This can help assess bony trauma from x-rays while determining the presence, extent, and severity of associated soft tissue problems involving muscles, joints, tendons, and blood vessels from MRI. Rapid detection of devastating vascular injuries can help in prompt triage and management decisions with limb- and life-saving

implications. For example, in non-hospital settings (military and natural disaster settings), the presence of extensive soft tissue injury or vascular complications will warrant expedited transport or triage for rapid treatment. A simultaneous and rapid spiral MRX will enable synergistic CT and MR with complementary information, perfect co-registration, and potentially multivariable pixel information.

Spiral MRX can be a game changer for on-site, out-of-hospital settings for rapid triage and management of suspected or known spinal injuries. Current workup is only possible in elaborate and expensive non-portable health care settings with plain film radiography and CT to delineate bony injuries and MR for detection of injuries to the spinal cord and nerves, as well as the vital supporting soft tissues such as ligaments, muscles and joints. Here portable MRX can rapidly provide on-site information not obtainable with either one when used separately. In cases of bullet wounds and other metal shrapnel, additional precautions are necessary to ensure that the magnetic field does not significantly move the object within the body. Studies on MR imaging of patients with gunshot wounds at 1 T field strength have shown that some bullets do rotate to align with the direction of the field [33]. The deflection force depends on the shape and material of the object, and is only significant for certain types, mainly steel. Weaker magnetic fields of MRX provide more favorable conditions for metal objects, and a feature based on interior MRI that allows z-direction selection of the field to parallel the object can further minimize deflection. The study also determined that heating of the bullet by the magnetic field was insignificant.

The proposed MRX system can alternatively work in the radiographic imaging mode, where two-dimensional radiography can provide information on bony alignment and fragments, while MRI adds the missing third dimension to radiographic information and provides information on injuries to spinal cord, nerves, and ligaments. Likewise, head injuries are a major cause for disability and deaths that can also be rapidly assessed with spiral MRX in non-hospital settings. It is well recognized that while CT is the modality of choice for injuries to the bony cranium and for acute intracranial hemorrhage, MR outperforms every other known imaging modality for evaluation of injury to brain parenchyma. Combining modalities with MRX will provide a one-stop, accurate, and rapid categorization of the presence and severity of head trauma and potentially mitigate some devastating outcomes of these injuries.

Beyond trauma, the applications of MRX may surpass those of the portable and mobile CT scanners that are limited to information of bone and hemorrhage. Here MRX can provide better information on the presence and severity of ischemic strokes and possibly other causes of acute neurological symptoms from insults to the brain parenchyma, as compared to rather limited information now generated with CT or with a stationary time-consuming MR examination in a healthcare setting. Evaluation of the heart with MRX will pose unique challenges to the temporal and spatial resolution of the combined imaging modalities. Although not insurmountable, technological blending of cardiac MR with invasive coronary angiogram (ICA with C-arm x-ray system) could lead to a single all-encompassing test where coronary stenosis with ICA can be simultaneously corroborated with its consequence on the myocardial function and perfusion under rest and/or stress with cardiac MR, thus overlaying the anatomic coronary compromise on top of functional myocardial damage. This as yet elusive one-stop imaging of the heart can lead to rapid decision-making in which sub-stenotic or non-critical lesions need to be aggressively stented (those with myocardial function or perfusion impairment in rest or drug induced stress on MRI). Furthermore, in post-stent or angioplasty events, MRX may even provide information on luminal patency and recovered or non-recovered myocardium.

Currently, coronary catheterization is the gold standard for luminal stenosis in ischemic heart disease. CT is useful to triage patients who can be safely discharged versus patients who need ICA with a C-arm x-ray assembly. MR is the gold standard for anything myocardial (congenital, inflammatory, neoplastic conditions), and most importantly for determining cardiac function and extent of damage as well as chances of salvaging myocardial function following revascularization (coronary artery bypass grafting or stent placement in coronary arteries). The case can also be made that MRX will obviate the need for high radiation dose CT since the structural information can be acquired at extremely low levels of radiation for evaluation of lungs and bones, and soft tissue information typically requiring higher dose CT can instead be "filled-in" with the superior contrast resolution of MR.

VI. CONCLUSION

In summary, the combination of spiral CT and MRI enables excellent spatial resolution and low-contrast resolution to be provided in a single scan. We have shown simulation results of realistic system designs for spiral MRX and a joint image reconstruction scheme. Permanent magnets will likely be used in our initial designs, though superconducting fibers are a promising possibility. A lightweight, low-power x-ray source will be utilized to minimize radiation dose in conjunction with a flat panel detector in a compact gantry. The spiral acquisition protocol allows a large coverage along the z-direction for both modalities. In addition to its widespread potential in hospital settings, the proposed MRX scanner has multiple niche applications such as imaging on disaster sites, in battle fields, and for under-developed regions.

REFERENCES

[1] G. Wang *et al.*, "Towards Omni-Tomography—Grand fusion of multiple modalities for simultaneous interior Tomography," *PLoS One*, vol. 7, no. 6, p. 39700, 2012.

[2] L. Gjesteby, M. Getzin, and G. Wang, "Low-field designs for interior MRI and CT coupling," in *Proc. Northeast Biomed. Eng. Conf. (NEBEC)*, 2015, pp. 1–2.

[3] G. Wang *et al.*, "Vision 20/20: Simultaneous CT-MRI—Next chapter of multimodality imaging," *Med. Phys.*, vol. 42, no. 10, pp. 5879–5889, 2015.

[4] V. R. Yelleswarapu, F. Liu, W. Cong, and G. Wang, "Top-level system designs for hybrid low-field MRI–CT with potential of pulmonary imaging," *Sens. Imag.*, vol. 15, no. 1, p. 98, Oct. 2014.

[5] Z. Wen, R. Fahrig, S. Conolly, and N. J. Pelc, "Investigation of electron trajectories of an X-ray tube in magnetic fields of MR scanners," *Med. Phys.*, vol. 34, no. 6, pp. 2048–2058, 2007.

[6] L. L. Tsai, R. W. Mair, M. S. Rosen, S. Patz, and R. L. Walsworth, "An open-access, very-low-field MRI system for posture-dependent ^{3}He human lung imaging," *J. Magn. Reson.*, vol. 193, no. 2, pp. 274–285, 2008.

[7] C. Z. Cooley *et al.*, "Two-dimensional imaging in a lightweight portable MRI scanner without gradient coils," *Magn. Reson. Med.*, vol. 73, pp. 872–883, 2015.

[8] H. Yu and G. Wang, "Compressed sensing based interior tomography," *Phys. Med. Biol.*, vol. 54, no. 9, p. 2791, 2009.

[9] G. Wang and H. Yu, "The meaning of interior tomography," *Phys. Med. Biol.*, vol. 58, no. 16, p. R161, 2013.

[10] R. Fahrig *et al.*, "A truly hybrid interventional MR/X-ray system: Feasibility demonstration," *J. Magn. Reson. Imag.*, vol. 13, no. 2, pp. 294–300, 2001.

[11] G. Wang and M. W. Vannier, "Low-contrast resolution in volumetric X-ray CT—Analytical comparison between conventional and spiral CT," *Med. Phys.*, vol. 24, no. 3, pp. 373–376, 1997.

[12] B. K. Halbach, L. Berkeley, U. C. Berkeley, and B. Ca, "Physical and optical properties of rare earth cobalt magnets," *Nucl. Instrum. Methods*, vol. 187, no. 1, pp. 109–117, 1981.

[13] R. Bjørk, C. R. H. Bahl, A. Smith, and N. Pryds, "Optimization and improvement of Halbach cylinder design," *J. Appl. Phys.*, vol. 104, no. 1, pp. 1–9, 2008.

[14] P. Suetens, *Fundamentals of Medical Imaging*. Cambridge, U.K.: Cambridge Univ. Press, 2009.

[15] P. Blümler, "Proposal for a permanent magnet system with a constant gradient mechanically adjustable in direction and strength," in *Proc. Concepts Magn. Reson. B Magn. Reson. Eng.*, 2016, pp. 41–48.

[16] M. D. Bird, I. R. Dixon, and J. Toth, "Design of the next generation of florida-bitter magnets at the NHMFL," *IEEE Trans. Appl. Supercond.*, vol. 14, no. 2, pp. 1253–1256, Jun. 2004.

[17] M. Ristic, Y. Gryska, J. V. M. McGinley, and V. Yufit, "Supercapacitor energy storage for magnetic resonance imaging systems," *IEEE Trans. Ind. Electron.*, vol. 61, no. 8, pp. 4255–4264, Aug. 2014.

[18] C. Liu, Z. Yu, D. Neff, A. Zhamu, and B. Z. Jang, "Graphene-based supercapacitor with an ultrahigh energy density," *Nano Lett.*, vol. 10, no. 12, pp. 4863–4868, 2010.

[19] T. Lin *et al.*, "Nitrogen-doped mesoporous carbon of extraordinary capacitance for electrochemical energy storage," *Science*, vol. 350, no. 6267, pp. 1508–1513, Dec. 2015.

[20] Y. Xi, J. Zhao, J. Bennett, M. Stacy, A. Sinusas, and G. Wang, "Simultaneous CT-MRI Reconstruction for Constrained Imaging Geometries using Structural Coupling and Compressive Sensing," *IEEE Trans. Biomed. Eng.*, vol. 63, no. 6, pp. 1301–1309, Jun. 2016.

[21] Y. Xi, Y. Chen, R. Tang, J. Sun, and J. Zhao, "United iterative reconstruction for spectral computed tomography," *IEEE Trans. Med. Imag.*, vol. 34, no. 3, pp. 769–778, Mar. 2015.

[22] B. Vandeghinste *et al.*, "Split-Bregman-based sparse-view CT reconstruction," in *Proc. 11th Int. Meeting Fully Three-Dimensional Image Reconstruction Radiol. Nucl. Med. (Fully 3D)*, 2011, pp. 431–434.

[23] B. Kladny, K. Glückert, B. Swoboda, W. Beyer, and G. Weseloh, "Comparison of low-field (0.2 Tesla) and high-field (1.5 Tesla) magnetic resonance imaging of the knee joint," *Arch. Orthopaedic Trauma Surgery*, vol. 114, no. 5, pp. 281–286, 1995.

[24] W. Mao and G. Wang, "TU-H-BRA-05: A system design for integration of an interior MRI and a linear accelerator," *Med. Phys.*, vol. 43, no. 6, p. 3769, 2016.

[25] G. Krainz, "Quench protection and powering in a string of superconducting magnets for the large hadron Collider," Geneva, Switzerland, Tech. Rep. CERN THESIS-2002-003, CERN 1997.

[26] R. Soika *et al.*, "Fabrication and prototype testing of a strain-tolerant Bi-2212 cable," *IEEE Trans. Appl. Supercond.*, vol. 11, no. 1, pp. 2142–2145, Mar. 2001.

[27] A. P. Drozdov, M. I. Eremets, I. A. Troyan, V. Ksenofontov, and S. I. Shylin, "Conventional superconductivity at 203 kelvin at high pressures in the sulfur hydride system," *Nature*, vol. 525, no. 7567, pp. 73–76, Sep. 2015.

[28] D. C. van der Laan, X. F. Lu, and L. F. Goodrich, "Compact $GdBa_2Cu_3O_7Ű\bar{o}$ coated conductor cables for electric power transmission and magnet applications," *Supercond. Sci. Technol.*, vol. 24, no. 4, p. 042001 (1-6), 2011.

[29] H. M. Jang, S. K. Lee, Y. W. Kim, and C. H. Ryu, "Superconducting cable," U.S. Patent 201 301 653 24, Jun. 27, 2013.

[30] D. Homa, Y. Liang, G. Pickrell, D. Homa, Y. Liang, and G. Pickrell, "Superconducting fiber," *Appl. Phys. Lett.*, vol. 103, no. 82601, pp. 1–4, 2013.

[31] D. Homa, Y. Liang, C. Hill, G. Kaur, and G. Pickrell, "Superconducting tin core fiber," *Appl. Phys. A Mater. Sci. Process.*, vol. 118, no. 1, pp. 23–26, 2014.

[32] D. Homa, G. Kaur, G. Pickrell, and Y. Liang, "Efficient cooling of superconducting fiber core via holey cladding," *Cryogenics*, vol. 61, pp. 25–30, 2014.

[33] E. Martinez-del-Campo, L. Rangel-Castilla, H. Soriano-Baron, and N. Theodore, "Magnetic resonance imaging in lumbar gunshot wounds: An absolute contraindication?" *Neurosurg. Focus*, vol. 37, no. 1, p. E13, 2014.

LARS GJESTEBY received the B.S. degree in biomedical engineering from the Rensselaer Polytechnic Institute, Troy, NY, USA, in 2014, where he is currently pursuing the Ph.D. degree in biomedical engineering under the supervision of G. Wang. His current research interests include x-ray computed tomography, metal artifact reduction, deep learning, and the combination of CT and MRI for simultaneous imaging.
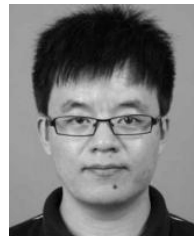
YAN XI received the Ph.D. degree from the Biomedical Engineering School, Shanghai Jiao Tong University, Shanghai, China, in 2013. He was a Post-Doctoral Research Fellow with the Biomedical Imaging Cluster, Rensselaer Polytechnic Institute. His interests include X-ray-computed tomography, x-ray phase-contrast imaging, and joint tomographic reconstruction.

MANNUDEEP K. KALRA received the M.D. degree from the Government Medical College and Hospital in India. He is currently Attending Radiologist with the Divisions of Thoracic and Cardiac Imaging, Massachusetts General Hospital, and an Associate Professor of Radiology with the Harvard Medical School. He also serves as the Director of the MGH Webster Center for Advanced Research and Education in Radiation. He has authored over 250 original research articles, book chapters, abstracts, and review articles, with a primary focus on CT radiation dose optimization and CT technology assessment. He has delivered over 100 national and international lectures and workshops on various aspects of CT technology and radiation dose. His work on CT radiation dose optimization has earned several awards and prizes at national and international radiology meetings.

QINGSONG YANG received the B.S. degree from the Department of Engineering Physics, Tsinghua University, Beijing, China, in 2013. He is currently pursuing the Ph.D. degree in biomedical engineering with the Rensselaer Polytechnic Institute under the supervision of G. Wang. His research interests include x-ray phase contrast imaging and photon-counting CT technology.

GE WANG (F'03) received the Ph.D. degree in ECE, University at Buffalo The State University of New York, Buffalo, NY, USA. He is currently the Clark and Crossan Endowed Chair Professor and the Director of the Biomedical Imaging Center, Rensselaer Polytechnic Institute, Troy, NY, USA. He authored the pioneering papers on the first spiral/helical cone-beam computed tomography (CT) algorithm in 1991. Spiral/helical cone-beam/multi-slice CT is constantly used in almost all hospitals worldwide. There are over 100 million CT scans yearly with a majority in the spiral/helical cone-beam/multi-slice mode. He and his collaborators published the first paper on bioluminescence tomography, creating a new area of optical molecular tomography. His group published the first papers on interior tomography and omni-tomography for grand fusion of all relevant tomographic modalities (all-in-one) to acquire different datasets simultaneously (all-at-once) with simultaneous CT-MRI as an example. His results were featured in Nature, Science, and PNAS, and recognized with academic awards. He published over 400 journal papers, some of which were highly cited. His team has been in collaboration with world-class groups, and continuously well-funded by federal agencies. His interest includes x-ray CT, optical molecular tomography, multimodality imaging, bibliometrics, and deep learning. He is a fellow of the SPIE, OSA, AIMBE, AAPM, and AAAS. He is the Lead Guest Editor of the four IEEE TRANSACTIONS ON MEDICAL IMAGING Special Issues on cone-beam CT, molecular imaging, compressive sensing, and spectral CT respectively, the founding Editor-in-Chief of the *International Journal of Biomedical Imaging*, and an Associate Editor of the IEEE TRANSACTIONS ON MEDICAL IMAGING, the IEEE ACCESS, *Medical Physics*, and the *Journal of X-ray Science and Technology*.

• • •